OPEN ACCESS

International
Journal
Of Modern Engineering Research (IJMER)

Implementation scheme of the Direct Torque Control strategy to Four Switch Three Phase Inverter fed Induction Motor drives

G. Chitra[1], P. R. Muralimohan[2]
[1]*PG Student (PE&ED) Department of Electrical & Electronics Engineering S.V.C.E.T., Chittoor*
[2]*Associate Professor Department of Electrical & Electronics Engineering S.V.C.E.T., Chittoor*

Abstract: *This paper proposes a novel direct torque control (DTC) strategy for induction motor (IM) drives fed by a four switch three-phase inverter (FSTPI). The introduced strategy is based on the emulation of the operation of the conventional six switch three-phase inverter (SSTPI). This has been achieved thanks to a suitable combination of the four unbalanced voltage vectors intrinsically generated by the FSTPI, leading to the synthesis of the six balanced voltage vectors of the SSTPI.*

This approach has been adopted in the design of the vector selection table of the proposed DTC strategy which considers a subdivision of the Clarke plane into six sectors. Simulation results have revealed that, thanks to the proposed DTC strategy, FSTPI-fed IM drives exhibit interesting performance. These have been experimentally validated and compared to the ones yielded by the Takahashi and the basic DTC strategies dedicated to the SSTPI and to the FSTPI, respectively.

I. Introduction

IN RECENT years, direct torque control (DTC) strategies of induction motor (IM) drives have been widely implemented in industrial variable speed applications. Introduced in the middle of the 1980s, the first DTC strategy involves a simple control scheme which makes it possible rapid real time implementation. Since then, several investigations carried out in order to improve the performance of the original DTC strategy.

The major focused features are the uncontrolled switching frequency of the inverter and the high torque ripple resulting from the use of flux and torque hysteresis controllers.

Currently and more than two decades of investigation, several DTC strategies have been proposed so far. These could be classified within four major categories: 1) strategies considering variable hysteresis band controllers 2) strategies with space vector modulation (SVM)-based control of the switching frequency 3) strategies using predictive control scheme and 4) strategies built around intelligent control approaches. Nevertheless, the gained performance is allied to significant increase of implementation schemes.

Commonly, the voltage source inverter (VSI) feeding IM under DTC is the six-switch three-phase inverter (SSTPI). This said, some applications such as electric and hybrid propulsion systems, should be as reliable as possible. Within this requirement, the reconfiguration of the SSTPI into a four-switch three-phase inverter (FSTPI), in case of a switch/leg failure, is currently given an increasing attention . A DTC strategy dedicated to FSTPI-fed IM drives has been proposed . In spite of its simplicity, this strategy is penalized by the low dynamic and the high ripple of the torque. These drawbacks are due to the application of unbalanced voltage vectors to control flux and torque with a subdivision of the Clarke plane limited to four sectors.

Recently, an attempt to discard the previously described disadvantages has been proposed where a DTC scheme using a 16-sector vector selection table has been implemented. Nevertheless, it has been noted that the drive performance remains relatively low due to the increase of the CPU time which is linked to the complexity of the involved vector selection table. In order to achieve a constant switching frequency and to decrease the torque ripple, many DTC schemes based on SVM, using the FSTPI as a VSI, dedicated to control induction and permanent-magnet synchronous motors have been reported in the literature . These strategies offer high performance in terms of torque ripple reduction allied to the control of the inverter switching losses. However, these performances are compromised by the complexity of their implementation schemes.

This paper proposes a new DTC strategy dedicated to FSTPI- fed IM drives. It is based on the emulation of the SSTPI operation thanks to the synthesis of an appropriate vector selection table, which is addressed by hysteresis controllers. The resulting simplicity of the implementation scheme makes the strategy very attractive in many applications, such as the automotive one.

II. DTC Of FSTPI-Fed IM Drives: Background

A. DTC Basis

DTC strategies allow a direct control of the motor variables through an appropriate selection of the inverter control signals, in order to fulfil the requirements as whether the stator flux and torque need to be increased, decreased, or maintained. These decisions are achieved according to the output $\mathbf{C}_{\emptyset}$ of the flux hysteresis controller, the output $\boldsymbol{C_\tau}$ of the torque hysteresis controller, and the angular displacement $\boldsymbol{\theta_s}$ of the stator flux vector $\boldsymbol{\Phi_s}$ in the Clarke ( ) plane.

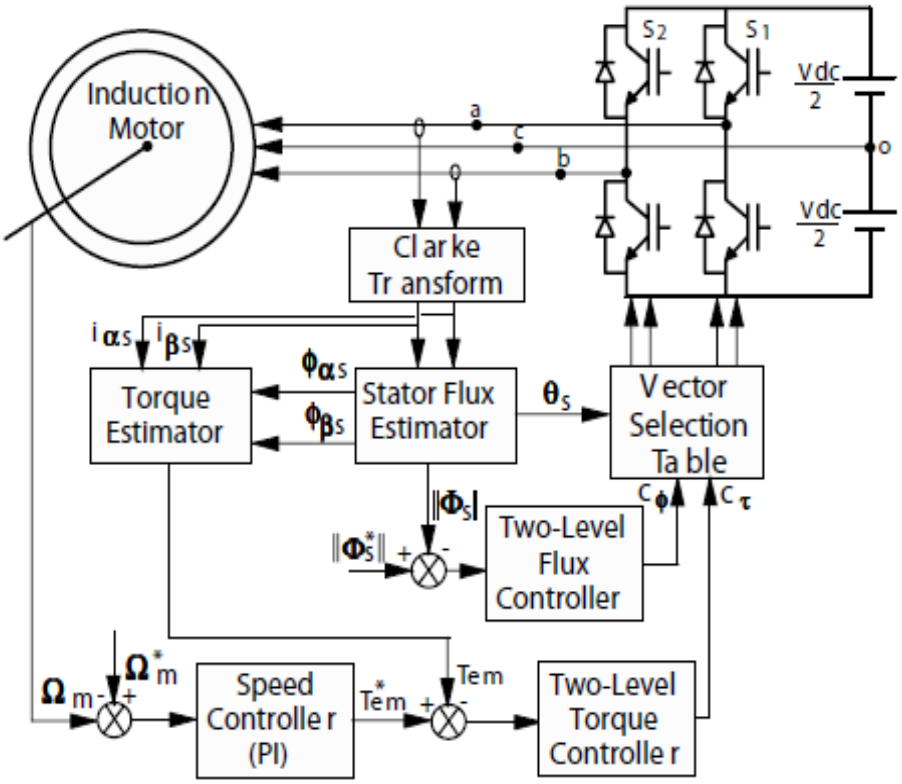

Fig.1. Implementation scheme of the DTC strategy dedicated to FSTPI-fed IM drives.

The dynamic of $\boldsymbol{\Phi_s}$ is governed by the stator voltage equation expressed in the stationary reference frame, as follows: $\frac{d}{dt}\boldsymbol{\Phi_s} = \mathbf{V_s} - \mathbf{r_s I_s}$

where **Vs , $\mathbf{I_s}$** , and rs are the stator voltage vector, current vector, and resistance, respectively. Neglecting the voltage drop $\mathbf{r_s}$ $\mathbf{I_s}$ across the stator resistance, and taking into account that the voltage vector is constant in each sampling period T_s , the variation of the stator flux vector turns to be proportional to the applied voltage vector. Maintaining the stator flux constant, the variation of the electromagnetic torque Tem depends on the direction of the applied voltage vector, such that:

$$\boldsymbol{T_{em} = N_P \frac{M}{l_s l_r - M^2} ||\Phi s|| ||\Phi_r^s|| \sin\delta}$$

where $\boldsymbol{\Phi_r^s}$ is the rotor flux vector referred to the stator, is the angular shift between the stator and rotor fluxes, **Np** is the pole pair number, and $\mathbf{I_s}$, $\mathbf{I_r}$, and M are the stator self-inductance, the rotor self-inductance, and the mutual inductance, respectively. The implementation scheme of the DTC strategy dedicated to a FSTPI-fed IM, shown in Fig. 1, has the same layout as the one of the basic DTC strategy initially proposed, except that,

1) the SSTPI inverter is reconfigured to a FSTPI. Such a reconfiguration is carried out by adding to the former three extra TRIACs with three fast acting fuses,

2) the three-level hysteresis controller in the torque loop is substituted by a two-level hysteresis controller. As will be depicted in Section III, this substitution is motivated by the fact that no zero voltage vector is involved in the proposed DTC scheme

TABLE I:

Switching states, Stator phase Voltages, their Clarke Components and their corresponding Voltage Vectors

(S_1S_2)	V_{as}	V_{bs}	V_{cs}	$V_{\alpha s}$	$V_{\beta s}$	V_1
(0 0)	$\frac{-V_{dc}}{6}$	$\frac{-V_{dc}}{6}$	$\frac{V_{dc}}{3}$	$\frac{-V_{dc}}{2\sqrt{6}}$	$\frac{-V_{dc}}{2\sqrt{2}}$	V_1
(1 0)	$\frac{V_{dc}}{2}$	$-\frac{V_{dc}}{2}$	0	$\frac{3V_{dc}}{2\sqrt{6}}$	$\frac{-V_{dc}}{2\sqrt{2}}$	V_2
(1 1)	$\frac{V_{dc}}{6}$	$\frac{V_{dc}}{6}$	$\frac{V_{dc}}{3}$	$\frac{V_{dc}}{2\sqrt{6}}$	$\frac{-V_{dc}}{2\sqrt{2}}$	V_3
(0 1)	$-\frac{V_{dc}}{2}$	$\frac{V_{dc}}{2}$	0	$-\frac{3V_{dc}}{2\sqrt{6}}$	$\frac{V_{dc}}{2\sqrt{2}}$	V_4

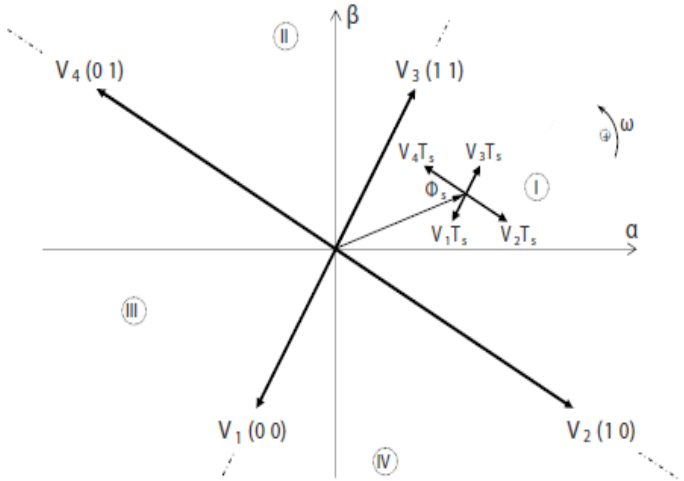

Fig.2 Unbalanced active voltage vectors generated by the FSTPI

B. Intrinsic Voltage Vectors of the FSTPI

The FSTPI topology consists of a two-leg inverter as illustrated in Fig. 1. Two among the three phases of the motor are connected to the FSTPI legs, while the third one is connected to the middle point of the dc-bus voltage.

Let us assume that the states of the four insulated-gate bipolar transistors (IGBTs) of the FSTPI are denoted by the binary variables S1 to S4 , where the binary "1" corresponds to an ON state and the binary "0" indicates an OFF state. The IM stator voltages are expressed in terms of the states (S1 and S2) of the upper IGBTs, as follows:

$$\begin{bmatrix} \mathbf{V_{as}} \\ \mathbf{V_{bs}} \\ \mathbf{V_{cs}} \end{bmatrix} = \frac{\mathbf{V_{dc}}}{6} \begin{bmatrix} \mathbf{4} & \mathbf{-2} & \mathbf{-1} \\ \mathbf{-2} & \mathbf{4} & \mathbf{-1} \\ \mathbf{-2} & \mathbf{-2} & \mathbf{2} \end{bmatrix} \begin{bmatrix} \mathbf{S_1} \\ \mathbf{S_2} \\ \mathbf{1} \end{bmatrix} \qquad (3)$$

The Clarke transform applied to the stator voltages yields:

$$\begin{bmatrix} \mathbf{V_{\alpha s}} \\ \mathbf{V_{\beta s}} \end{bmatrix} = \sqrt{\frac{2}{3}} \begin{bmatrix} \mathbf{1} & -\frac{\mathbf{1}}{\mathbf{2}} & -\frac{\mathbf{1}}{\mathbf{2}} \\ \mathbf{0} & \frac{\sqrt{\mathbf{3}}}{\mathbf{2}} & -\frac{\sqrt{\mathbf{3}}}{\mathbf{2}} \end{bmatrix} \begin{bmatrix} \mathbf{V_{as}} \\ \mathbf{V_{bs}} \\ \mathbf{V_{cs}} \end{bmatrix} \qquad (4)$$

Four combinations of the states of the upper IGBTs are characterized by four active voltage vectors (V1 to V4) in the αβ plane, which are given in Table I.

Fig.2 shows the four active voltage vectors represented in the αβ plane. These vectors have unbalanced amplitudes and are shifted by an angle of $\pi/(2)$. Indeed, vectors V1 and V3 have an amplitude of Vdc/ √ 6, while vectors V2 and V4 have amplitude of Vdc/√2

TABLE II

Vector selection table of the basic DTC strategy

$C_\emptyset$ / C_r	+1 / +1	+1 / -1	-1 / +1	-1 / -1
Sector I	V_3	V_2	V_4	V_1
Sector II	V_4	V_3	V_1	V_2
sector III	V_1	V_4	V_2	V_3
Sector IV	V_2	V_1	V_3	V_4

C. Limitations of the Basic DTC of a FSTPI-Fed Induction Motor:

The basic DTC of an IM fed by the FSTPI is based on the subdivision of the αβ plane into four sectors, limited by the four active voltage vectors as shown in Fig. 2. The vector selection table corresponding to the basic strategy is presented in Table II.

Accounting for the symmetry of the four sectors, the following analysis of the torque and flux variations, will be limited to sector I, considering two cases:

1) the initial stator flux vector Φs1 is held by vector V_2 ;

2) the initial stator flux vector Φs1 is held by vector V_3 .

Equation (1) could be rewritten as follows:

$$\boldsymbol{\Phi_{s2}^{i} = \Phi_{s1} + (V_i - r_s I_s)T_s} \qquad (5)$$

Where V_i ($1 \leq i \leq 4$) is the voltage vector generated by the FSTPI.

Fig. 3 shows different phasor diagrams of (5), considering both cases previously cited with four scenarios selected from the vector selection table, for each. One can notice the following remarks which deal with the torque dynamic:

1) The application of voltage vectors $\boldsymbol{V_1}$ or $\boldsymbol{V_3}$ leads to a low torque dynamic if:

a) $\boldsymbol{\Phi_{s1}}$ is close to vector $\boldsymbol{V_2}$ due to the low amplitude $\boldsymbol{V_1}$ and $\boldsymbol{V_3}$ [see Fig. 3(a1) and (a3)];

b) $\boldsymbol{\Phi_{s1}}$ is close to vector $\boldsymbol{V_3}$ due to the low angular shift of the flux vector [see Fig. 3(b1) and (b3)]. It is to be noted that the torque command $\boldsymbol{C_\tau}$ of the control combinations ($\mathbf{C}_\emptyset = -1$, $\boldsymbol{C_\tau} = +1$) corresponding to sector II and ($\mathbf{C}_\emptyset = +1$, $\boldsymbol{C_\tau} = +1$) corresponding to sector I could not be achieved by the application of vectors $\boldsymbol{V_1}$ and $\boldsymbol{V_3}$, respectively.

2) The application of voltage vectors $\boldsymbol{V_2}$ or $\boldsymbol{V_4}$ leads to a low torque dynamic if $\boldsymbol{\Phi_{s1}}$ is close to vector $\boldsymbol{V_2}$ due to the low angular shift of the flux vector [see Fig. 3(a2) and (a4)]. One can notice that the control combinations ($\mathbf{C}_\emptyset = +1$, $\boldsymbol{C_\tau} = +1$) corresponding to sector IV and ($\mathbf{C}_\emptyset = -1$, $\boldsymbol{C_\tau} = +1$) corresponding to sector I could not be achieved with the application of voltage vectors $\boldsymbol{V_2}$ and $\boldsymbol{V_4}$, respectively.

3) The application of voltage vectors $\boldsymbol{V_2}$ or $\boldsymbol{V_4}$ leads to a high torque dynamic if $\boldsymbol{\Phi_{s1}}$ is located near vector $\boldsymbol{V_3}$ [see Fig. 3(b2) and (b4)].

From the previous analysis, one can clearly notice that the basic DTC strategy presents different limitations. These could be eradicated considering the introduced DTC strategy which will be developed in the following section.

PROPOSED DTC STRATEGY

A. Approach to Generate Balanced Voltages by the FSTPI

The proposed DTC strategy is based on the emulation of SSTPI operation by the FSTPI. This has been achieved through the generation of six balanced voltage vectors using the four intrinsic ones of the FSTPI. The generated vectors have the same amplitude and angular shift as those of the SSTPI. Basically, the active voltage vectors $\mathbf{V_k}$, with $1 \leq k \leq 6$, yielded by the SSTPI have an amplitude $\mathbf{V_k}$ equal to $\sqrt{(2/3)}\ \mathbf{V_{dc}}$, where $\mathbf{V_{dc}}$ is the dc-bus voltage. For the same value of $\mathbf{V_{dc}}$, the voltage vectors $\boldsymbol{V_i}$, with $1 \leq i \leq 4$, generated by the FSTPI, present unbalanced amplitudes $\boldsymbol{V_i}$, such that:

$$\begin{cases} \mathbf{V_1} = \mathbf{V_3} = \frac{\mathbf{V_{dc}}}{\sqrt{6}} = \frac{1}{2}\mathbf{V_k} \\ \mathbf{V_2} = \mathbf{V_4} = \frac{\mathbf{V_{dc}}}{\sqrt{2}} = \frac{\sqrt{3}}{2}\mathbf{V_k} \end{cases} \qquad \mathbf{(6)}$$

therefore, a dual application of the voltage vector $\mathbf{V_1}$ (respectively, $\mathbf{V_3}$) of the FSTPI, leads to the generation of the voltage vector $\mathbf{V_{11}}$ (respectively, $\mathbf{V_{33}}$), as shown in Fig. 4. It is to be noted that $\mathbf{V_{11}}$ and $\mathbf{V_{33}}$ are identical to two vectors among the six generated by the SSTPI. Now, let us call Vij the voltage vectors

resulting from the sums of successive voltage vectors Vi and Vj , with $1 \le i \le 4$ and $1 \le j \le 4$. As far as the angular shift between two successive voltage vectors is equal to $\pi/2$, the amplitude $\mathbf{V_{ij}}$ of vectors $\mathbf{V_{ij}}$ can be expressed as follows:

$$\mathbf{V_{ij}} = \sqrt{\mathbf{V_i^2} + \mathbf{V_j^2}} = \sqrt{\frac{\mathbf{1}}{\mathbf{6}} + \frac{\mathbf{1}}{\mathbf{2}}\mathbf{V_{dc}}} = \sqrt{\frac{\mathbf{2}}{\mathbf{3}}}\mathbf{V_{dc}} = \mathbf{V_k} \quad \textbf{(7)}$$

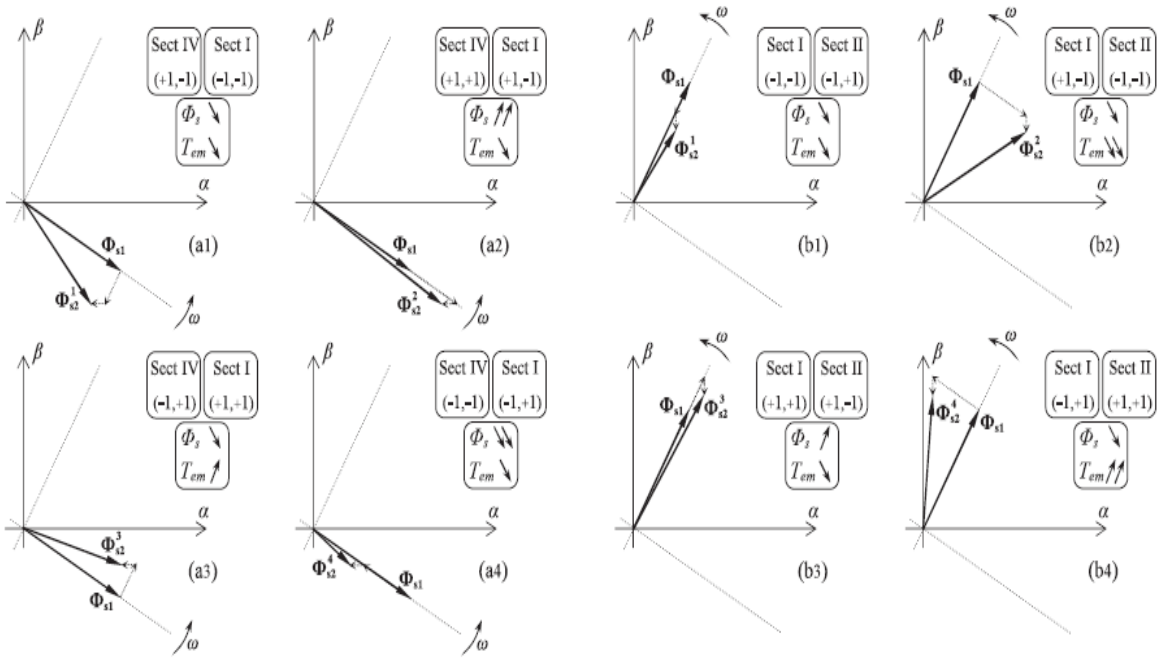

Fig. 3. Phasor diagrams describing the evolution of the stator flux vector in the case where it is located in the limits of sector I. Legend: (a) initial flux vector □ s1 held by the voltage vector V2 (b) initial flux vector □ s1 held by the voltage vector V3.

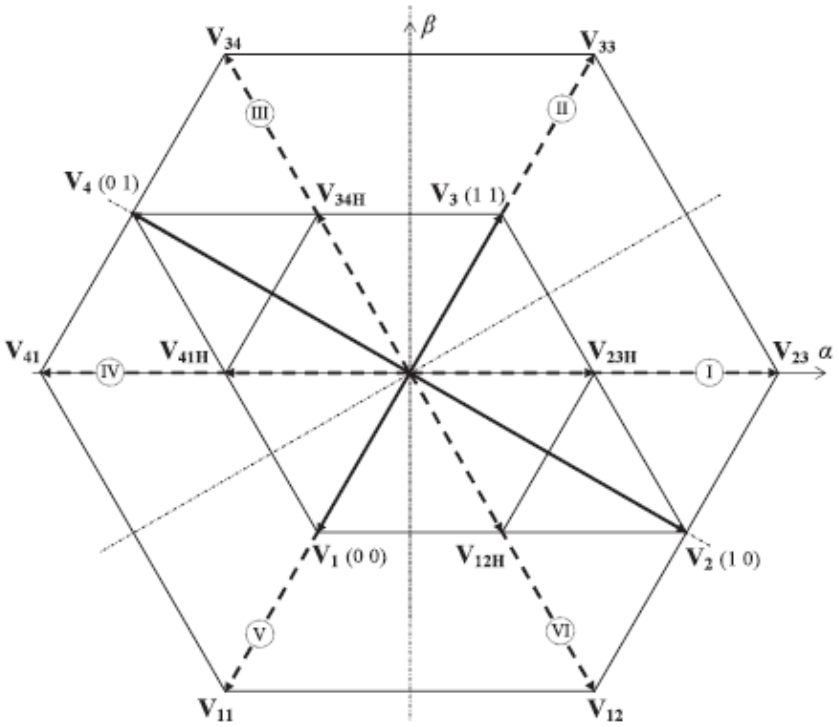

.Fig.4. Generation of the SSTPI active voltage vectors using the four unbalanced voltage ones of the FSTPI

One can notice that the voltage vectors Vij have the same amplitude as the ones generated by the SSTPI. Beyond the amplitude, the four generated vectors, named $\mathbf{V_{12}}$, $\mathbf{V_{23}}$, $\mathbf{V_{34}}$, and $\mathbf{V_{41}}$, as shown in Fig. 4, share the same phases with the four remaining active voltage vectors of the SSTPI. Table III summarizes the Clarke components of the six voltage vectors generated by the FSTPI considering the previously described approach.

TABLE III
Clarke COMPONENTS OF THE GENERATED VOLTAGE VECTORS

$\mathbf{V_{ij}}$	$\mathbf{V_{23}}$	$\mathbf{V_{33}}$	$\mathbf{V_{34}}$	$\mathbf{V_{41}}$	$\mathbf{V_{11}}$	$\mathbf{V_{12}}$
$\mathbf{V_{\alpha s}}$	$\sqrt{\frac{2}{3}}V_{dc}$	$\frac{V_{dc}}{\sqrt{6}}$	$\frac{-V_{dc}}{\sqrt{6}}$	$-\sqrt{\frac{2}{3}}V_{dc}$	$\frac{-V_{dc}}{\sqrt{6}}$	$\frac{V_{dc}}{\sqrt{6}}$
$\mathbf{V_{\beta s}}$	0	$\frac{V_{dc}}{\sqrt{2}}$	$\frac{V_{dc}}{\sqrt{2}}$	0	$-\frac{V_{dc}}{\sqrt{2}}$	$-\frac{V_{dc}}{\sqrt{2}}$

Following the generation of six balanced active voltage vectors ($\mathbf{V_{23}}$, $\mathbf{V_{33}}$, $\mathbf{V_{34}}$, $\mathbf{V_{41}}$, $\mathbf{V_{11}}$, and $\mathbf{V_{12}}$), the αβ plane turns to be subdivided into six symmetric sectors as illustrated in Fig. 4. Moreover, zero voltage vectors can be achieved through the application of two opposite intrinsic ones. The previously described approach represents a great control benefit so far as several DTC strategies implemented in SSTPI fed IM drives could be applied to FSTPI-fed IM ones.

B. Vector Selection Table of the Proposed DTC Strategy

The proposed DTC strategy is inspired from the earlier one introduced by Takahashi [1]. For the sake of reduction of the switching frequency as well as the torque ripple, the control combinations ($\mathbf{C_{\emptyset}}$ = ±1, $\boldsymbol{C_{\tau}}$ = 0) are omitted using a two-level hysteresis controller in the torque loop.

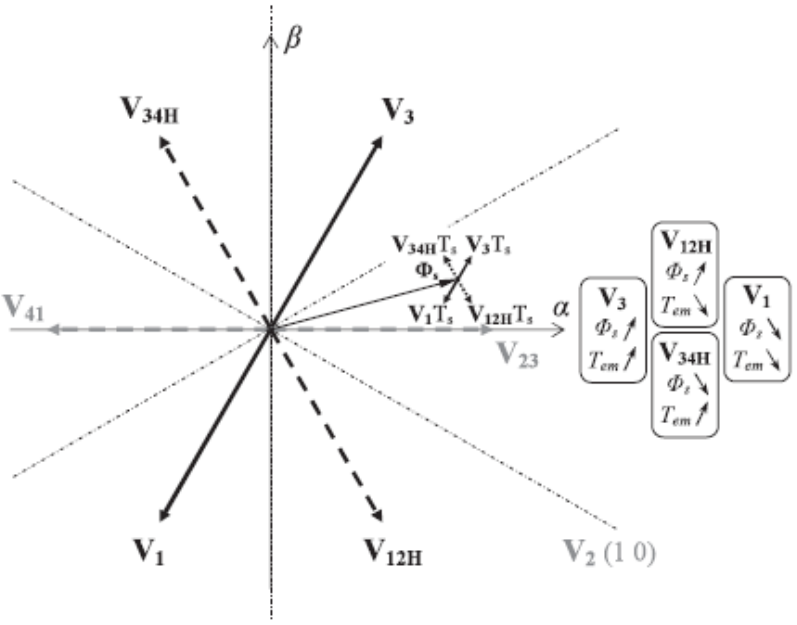

Fig. 5 Applied voltage vectors in the case where Φ_s is located in sector I.

The synthesis of the vector selection table of the proposed DTC strategy is based on the approach described in the previous paragraph. how the control combinations ($\mathbf{C_{\emptyset}}$=±1, $\boldsymbol{C_{\tau}}$= ±1) could be achieved applying the generated balanced voltage vectors?.

1) The application of $\mathbf{V_{11}}$ (respectively , $\mathbf{V_3}$) during two successive sampling periods $2\mathbf{T_s}$ allows the generation of $\mathbf{V_{11}}$ (respectively, $\mathbf{V_{33}}$),

2) The application of two consecutive voltage vectors $\mathbf{V_i}$ and $\mathbf{V_j}$ during two successive sampling periods leads to the generation of $\mathbf{V_{ij}}$.

As a result, the equivalent voltage vectors per sampling period $\mathbf{T_s}$ generated by the FSTPI, considering the adopted approach, can be expressed as:

$$\begin{cases} \mathbf{V_{11}\,H} = \frac{1}{2}\,\mathbf{V_{11}} = \mathbf{V_i} \\ \mathbf{V_{33}\,H} = \frac{1}{2}\,\mathbf{V_{33}} = \mathbf{V_3} \\ \mathbf{V_{ij}\,H} = \frac{1}{2}\,\mathbf{V_{ij}} \end{cases} \qquad (8)$$

where subscript H indicates the half of the corresponding voltage vector. In what follows, the synthesis of the vector selection table will be limited to sector I ($-\pi/6 \le \theta s \le \pi/6$). In this case and as shown in Fig. 5, the following voltage vectors are applied during a sampling period, according to the corresponding control combinations:

$$\begin{cases} \mathbf{V_3} \ \ \mathbf{for}\ (\mathbf{C_\emptyset} = +1\,, \boldsymbol{C_\tau} = +1) \\ \mathbf{V_{12}} \ \ \mathbf{for}(\mathbf{C_\emptyset} = +1, \boldsymbol{C_\tau} = -1) \\ \mathbf{V_{34}} \ \ \mathbf{for}(\mathbf{C_\emptyset} = -1, \boldsymbol{C_\tau} = +1) \\ \mathbf{V_1} \ \ \mathbf{for}(\mathbf{C_\emptyset} = -1, \boldsymbol{C_\tau} = -1) \end{cases}$$

In order to emulate the operation of the SSTPI, each control combination ($\mathbf{C_\emptyset}$, $\boldsymbol{C_\tau}$) should be maintained during two sampling periods 2Ts , which yields the application of:

$$\begin{cases} \mathbf{V_{33}} \ \mathbf{for}(\mathbf{C_\emptyset} = +1\,, \boldsymbol{C_\tau} = +1) \Rightarrow \mathbf{V_3\ then\ V_3} \\ \mathbf{V_{12}} \ \ \mathbf{for}(\mathbf{C_\emptyset} = +1, \boldsymbol{C_\tau} = -1) \Rightarrow \mathbf{V_1\ then\ V_2} \\ \mathbf{V_{34}} \ \ \mathbf{for}(\mathbf{C_\emptyset} = -1, \boldsymbol{C_\tau} = +1) \Rightarrow \mathbf{V_3\ then\ V_4} \\ \mathbf{V_{11}} \ \ \mathbf{for}(\mathbf{C_\emptyset} = -1, \boldsymbol{C_\tau} = -1) \Rightarrow \mathbf{V_1\ then\ V_1} \end{cases}$$

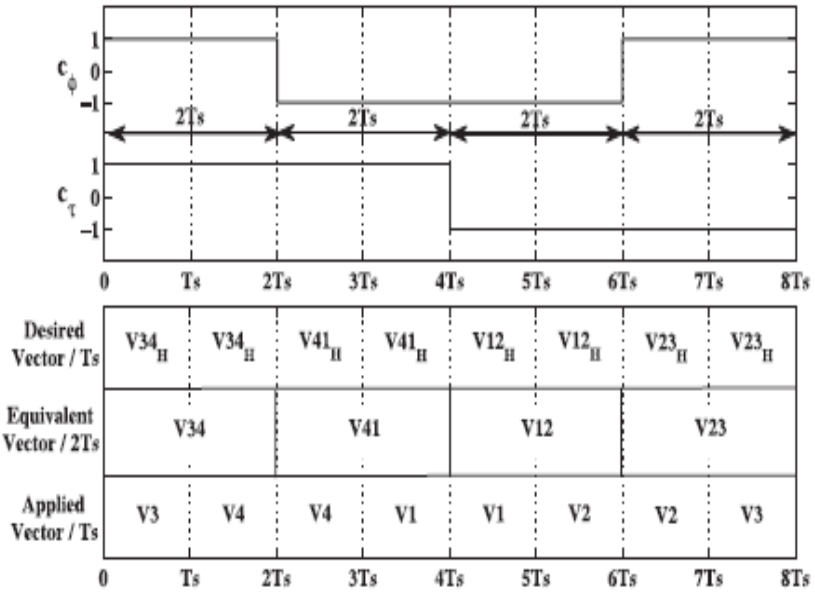

Fig. 6. Control combinations (c □ , c □), desired voltage vectors per Ts , equivalent voltage vectors during 2Ts , and applied voltage vectors per Ts

TABLE IV

DESIRED VECTOR SELECTION TABLE

$\boldsymbol{C_\emptyset}$ / $\boldsymbol{C_r}$	+1 / +1	+1 / -1	-1 / +1	-1 / -1
Sector I	$\mathbf{V_3}$	$\mathbf{V_{12H}}$	$\mathbf{V_{34H}}$	$\mathbf{V_1}$
Sector II	$\mathbf{V_{34H}}$	$\mathbf{V_{23H}}$	$\mathbf{V_{41H}}$	$\mathbf{V_{12H}}$
Sector III	$\mathbf{V_{41H}}$	$\mathbf{V_3}$	$\mathbf{V_1}$	$\mathbf{V_{23H}}$
Sector IV	$\mathbf{V_1}$	$\mathbf{V_{34H}}$	$\mathbf{V_{12H}}$	$\mathbf{V_3}$
Sector V	$\mathbf{V_{12H}}$	$\mathbf{V_{41H}}$	$\mathbf{V_{23H}}$	$\mathbf{V_{34H}}$
Sector VI	$\mathbf{V_{23H}}$	$\mathbf{V_1}$	$\mathbf{V_3}$	$\mathbf{V_{41H}}$

TABLE V

IMPLEMENTED VECTOR SELECTION TABLE

c_ϕ / c_τ	$+1$ / $+1$		$+1$ / -1		-1 / $+1$		-1 / -1	
Periods T_s	1^{st}	2^{nd}	1^{st}	2^{nd}	1^{st}	2^{nd}	1^{st}	2^{nd}
Sector I	$\mathbf{V_3}$		$\mathbf{V_1}$	$\mathbf{V_2}$	$\mathbf{V_3}$	$\mathbf{V_4}$	$\mathbf{V_1}$	
Sector II	$\mathbf{V_3}$	$\mathbf{V_4}$	$\mathbf{V_2}$	$\mathbf{V_3}$	$\mathbf{V_4}$	$\mathbf{V_1}$	$\mathbf{V_1}$	$\mathbf{V_2}$
Sector III	$\mathbf{V_4}$	$\mathbf{V_1}$	$\mathbf{V_3}$		$\mathbf{V_1}$		$\mathbf{V_2}$	$\mathbf{V_3}$
Sector IV	$\mathbf{V_1}$		$\mathbf{V_3}$	$\mathbf{V_4}$	$\mathbf{V_1}$	$\mathbf{V_2}$	$\mathbf{V_3}$	
Sector V	$\mathbf{V_1}$	$\mathbf{V_2}$	$\mathbf{V_4}$	$\mathbf{V_1}$	$\mathbf{V_2}$	$\mathbf{V_3}$	$\mathbf{V_3}$	$\mathbf{V_4}$
Sector VI	$\mathbf{V_2}$	$\mathbf{V_3}$	$\mathbf{V_1}$		$\mathbf{V_3}$		$\mathbf{V_4}$	$\mathbf{V_1}$

The inputs ($\mathbf{C_\emptyset}$, $\mathbf{C_\tau}$, and $\boldsymbol{\theta_s}$) of the vector selection table should be maintained during 2Ts which yields the implemented vector selection table provided in Table V. It is to be noted that both intrinsic and compounded voltage vectors are involved in sectors I, III, IV, and VI, while in sectors II and V, only the compounded voltage vectors are applied. Thus, one can expect an increase of the switching frequency in sectors II and V, with respect to the one in the remaining sectors.

TABLE VI: RATIO OF THE AMPLITUDES HARMONICS WITH RESPECT TO FUNDAMENTAL ONE

Harmonic	i_{as}			i_{cs}		
	2^{nd}	3^{rd}	5^{th}	2^{nd}	3^{rd}	5^{th}
$f_s = 2.5HZ$	8%	13.8%		9.5%	11%	
$f_s = 20HZ$	12%	13%	12.5%	7%	4%	8.5%

TABLE VII

INDUCTION MACHINE RATINGS

Power	**0.37 KW**	**Efficiency**	**77%**
Voltage	**230V/400V**	**Current**	**1.7A/1A**
Torque	**2.56 N.m**	**Stator Flux (Rms)**	**640 wb**
Speed	**1380 rpm**	**Frequency**	**50 HZ**

Simulation circuit:

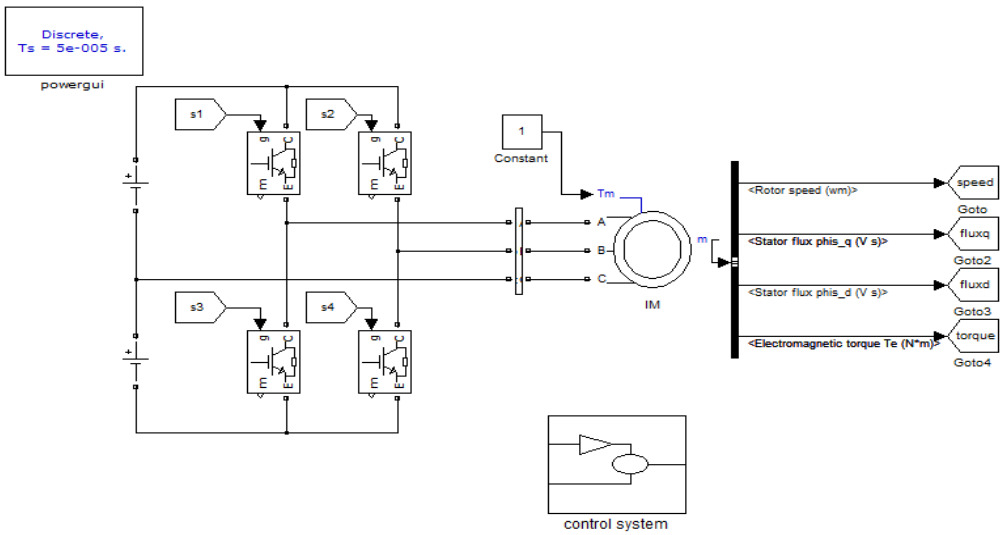

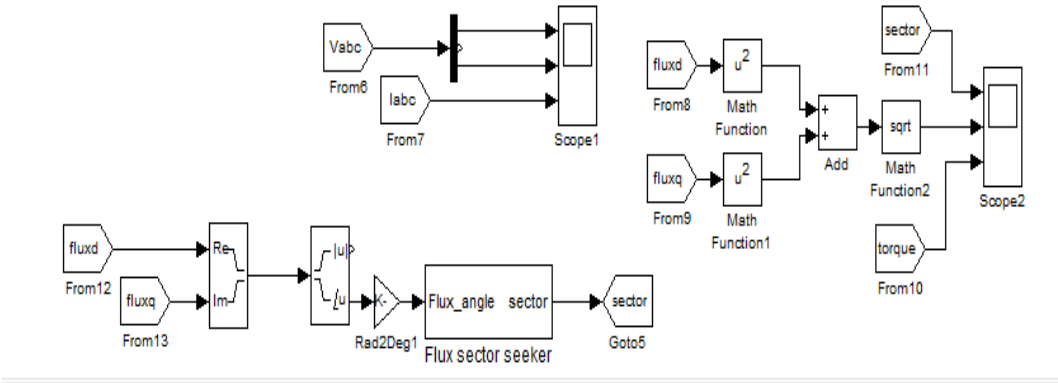

Simulation results:

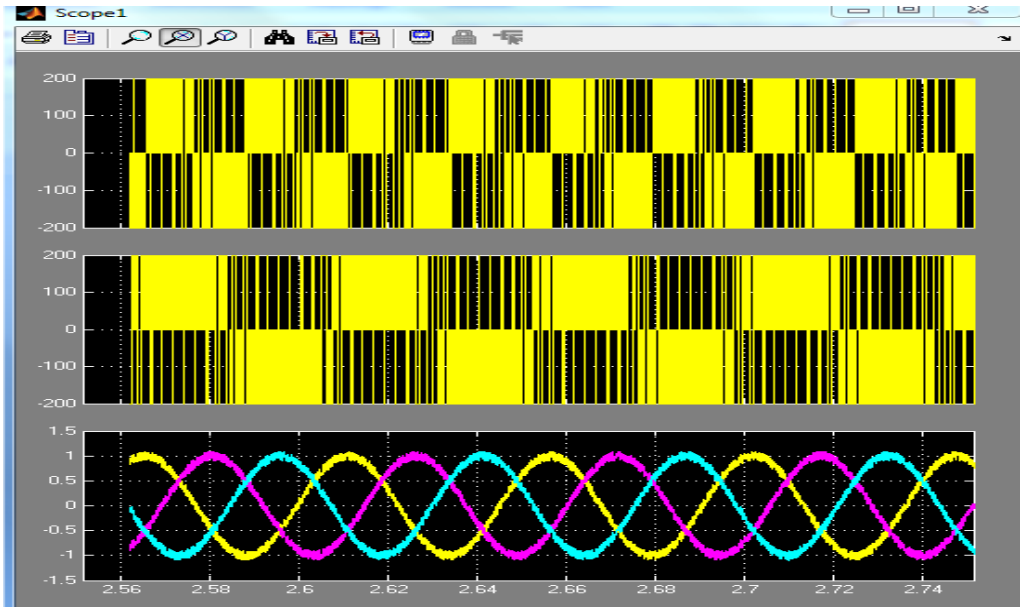

Fig: Stator a-phase voltage , Stator c-phase voltage, Stator phase currents

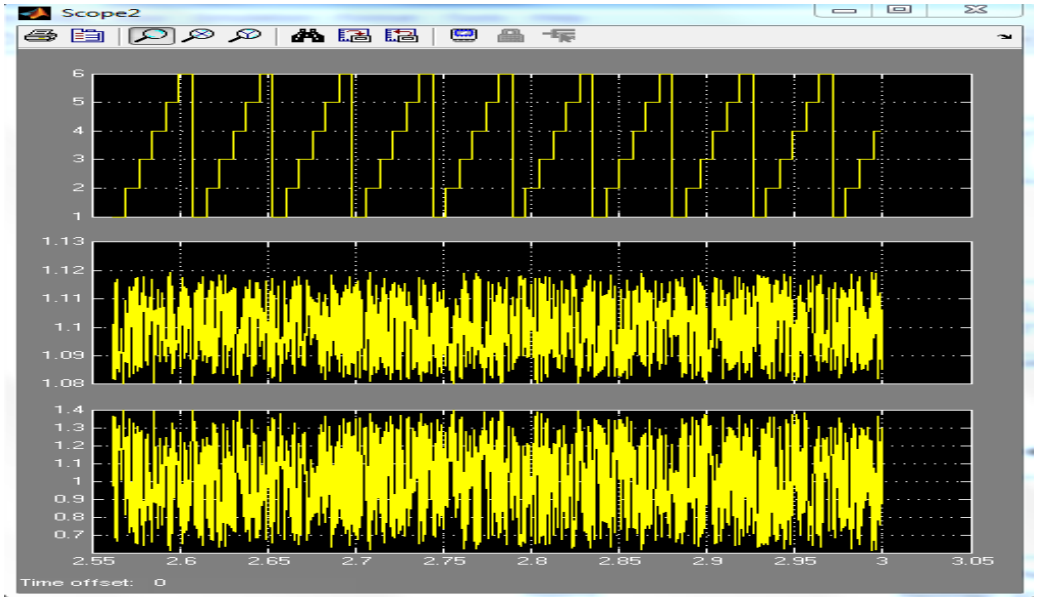

Fig: Sector section described in alpha,beta plane,stator flux amplitude and its reference and electromagnetic torque

III. Conclusion

This paper dealt with a new DTC strategy dedicated to FSTPI fed IM drives. The proposed DTC strategy is based on the emulation of the operation of the conventional SSTPI. This has been achieved thanks to suitable combinations of the four unbalanced voltage vectors intrinsically generated by the FSTPI, leading to the synthesis of the six balanced voltage vectors yielded by the SSTPI. This approach has been adopted in the design of the vector selection table which is simply addressed by hysteresis controllers, considering a subdivision of the Clarke plane into six sectors.

Simulation-based investigations of the IM steady-state features have revealed the high performance of the introduced DTC strategy. These performances have been the subject of an experimental validation along with a comparison against those yielded by Takahashi and the basic DTC strategies dedicated to the SSTPI and to the FSTPI, respectively.

REFERENCES

[1] I. Takahashi and T. Noguchi, "A new quick-response and high-efficiency control strategy of an induction motor," IEEE Trans. Ind. Appl., vol. 22, no. 5, pp. 820–827, Sep. 1986.

[2] Y. Zhang and J. Zhu, "Direct torque control of permanent magnet synchronous motor with reduced torque ripple and commutation frequency," IEEE Trans. Power Electron., vol. 26, no. 1, pp. 235–248, Jan. 2011.

[3] Y. Zhang, J. Zhu, Z. Zhao, W. Xu, and D. G. Dorrell, "An improved direct torque control for three-level inverter-fed induction motor sensor-less drive," IEEE Trans. Power Electron., vol. 27, no. 3, pp. 1502–1513, Mar.2012.

[4] A. Taheri, A. Rahmati, and S. Kaboli, "Efficiency improvement in DTC of six-phase induction machine by adaptive gradient descent of flux," IEEE Trans. Power Electron., vol. 27, no. 3, pp. 1552–1562, Mar. 2012.

[5] A. B. Jidin, N. R. B. N. Idris, A. H. B. M. Yatim, M. E. Elbuluk, and T. Sutikno, "A wide-speed high torque capability utilizing over modulation strategy in DTC of induction machines with constant switching frequency controller," IEEE Trans. Power Electron., vol. 27, no. 5, pp. 2566–2575, May 2012.

[6] J. K.Kang, D. W. Chung, and S. K. Sul, "Direct torque control of induction machine with variable amplitude control of flux and torque hysteresis bands," in Proc. Int. Elect. Mach. Drives Conf., Seattle, Washington, May 1999, pp. 640–642.

[7] K. B. Lee and F. Blaabjerg, "Sensor less DTC-SVM for induction motor driven by a matrix converter using a parameter estimation strategy," IEEE Trans. Ind. Electron., vol. 55, no. 2, pp. 512–521, Feb. 2008.

[8] Z. Zhifeng, T. Renyuyan, B. Boadong, and X. Dexin, "Novel direct torque control based on space vector modulation with adaptive stator flux observer for induction motors," IEEE Trans. Magn., vol. 48, no. 8, pp. 3133–3136, Aug. 2010.

[9] J. Beerten, J. Verveckken, and J. Driesen, "Predictive direct torque control for flux and torque ripple reduction," IEEE Trans. Ind. Electron., vol. 57, no. 1, pp. 404–412, Jan. 2010.

[10] T. Geyer, "Computationally efficient model predictive direct torque control," IEEE Trans. Power Electron., vol. 26, no. 10, pp. 2804–2816, Oct. 2011.

[11] H. Zhu, X. Xiao, and Y. Li, "Torque ripple reduction of the torque predictive control scheme for permanent-magnet synchronous motors," IEEE Trans. Ind. Electron., vol. 59, no. 2, pp. 871–877, Feb. 2012.

[12] S. K. Sahoo, S. Dasgupta, S. K. Panda, and J. X. Xu, "A Lyapunov function-based robust direct torque controller for a switched reluctance motor drive system," IEEE Trans. Power Electron., vol. 27, no. 2, pp. 555–564, Feb. 2012.

[13] M. N. Uddin and M. Hafeez, "FLC-based DTC scheme to improve the dynamic performance of an IM drive," IEEE Trans. Ind. Appl., vol. 48, no. 2, pp. 823–831, Mar./Apr. 2012.

[14] M. B. R. Correa, C. B. Jacobina, E. R. C. da Silva, and A. M. N. Lima, "A general PWM strategy for four-switch three-phase inverters," IEEE Trans. Power Electron., vol. 21, no. 6, pp. 1618–1627, Nov. 2006.

[15] K. D. Hoang, Z. Q. Zhu, andM. P. Foster, "Influence and compensation of inverter voltage drop in direct torque-controlled four-switch three-phase PM brushless AC drives," IEEE Trans. Power Electron., vol. 26, no. 8, pp. 2343–2357, Aug. 2011.

[16] R. Wang, J. Zhao, and Y. Liu, "A comprehensive investigation of fourswitch three-phase voltage source inverter based on double fourier integral analysis," IEEE Trans. Power Electron., vol. 26, no. 10, pp. 2774–2787, Oct. 2011.

[17] M. Azab and A. L. Orille, "Novel flux and torque control of induction motor drive using four switch three phase inverter," in Proc. IEEE Annu. Conf. Ind. Electron. Soc., Denver, CO, Nov./Dec. 2001, vol. 2, pp. 1268– 1273.

[18] B. Bouzidi, B. El Badsi, and A. Masmoudi, "Investigation of the performance of aDTCstrategy dedicated to the control ofB4 fed induction motor drives," Comput. Math. Elect. Electron. Eng., vol. 31, no. 1, pp. 224–236, 2012.

[19] D. Swierczynski, P. Kazinierkowski, and F. Blaabjerg, "DSP based direct torque control of permanent magnet synchronous motor (PMSM) using space vector modulation (DTC-SVM)," in Proc. IEEE Int. Symp. Ind. Electron., Aquila, Italy, Jul. 2002, vol. 3, pp. 723–727.

[20] S. Kazemlou and M. R. Zolghadri, "Direct torque control of four-switch three phase inverter fed induction motor using a modified SVM to compensate DC-link voltage imbalance," in Proc. IEEE Int. Conf. Electr. Power Energy Convers. Syst., Sharjah, UAE, Nov. 2009, pp. 1–6.

[21] Q. T. An, L. Z. Sun, K. Zhao, and L. Sun, "Switching function modelbased fast-diagnostic method of open-switch faults in inverters without sensors," IEEE Trans. Power Electron., vol. 26, no. 1, pp. 119–126, Jan. 2011.

[22] R. R. Errabelli and P. Mutschler, "Fault-tolerant voltage source inverter for permanent magnet drives," IEEE Trans. Power Electron., vol. 27, no. 2, pp. 500–508, Feb. 2012.

[23] M. D. Hennen, M. Niessen, C. Heyers, H. J. Brauer, and R. W. De Doncker, "Development and control of an integrated and distributed inverter for a fault tolerant five-phase switched reluctance traction drive," IEEE Trans. Power Electron., vol. 27, no. 2, pp. 547–554, Feb. 2012.

[24] U. M. Choi, H. G. Jeong, K. B. Lee, and F. Blaabjerg, "Method for detecting an open-switch fault in a grid-connected NPC inverter system," IEEE Trans. Power Electron., vol. 27, no. 6, pp. 2726–2739, Jun.